Langmuir
Article
pubs.acs.org/Langmuir

Spin-Assisted Layer-by-Layer Assembly: Variation of Stratification as Studied with Neutron Reflectivity†

Eugenia Kharlampieva,‡ Veronika Kozlovskaya,‡ Jennifer Chan,‡ John F. Ankner,§ and Vladimir V. Tsukruk*,‡

‡Department of Materials Science and Engineering, Georgia Institute of Technology, Atlanta, Georgia 30332, and §Spallation Neutron Source, Oak Ridge National Laboratory, Oak Ridge, Tennessee 37831

Received April 20, 2009. Revised Manuscript Received June 10, 2009

We apply neutron reflectivity to probe the internal structure of spin-assisted layer-by-layer (SA-LbL) films composed of electrostatically assembled polyelectrolytes. We find that the level of stratification and the degree of layer intermixing can be controlled by varying the type and concentration of salt during SA-LbL assembly. We observe well-defined layer structure in SA-LbL films when deposited from salt-free solutions. These films feature 2-nm-thick bilayers, which are ~3-fold thicker than those in conventional LbL films assembled under similar conditions. The addition of a 10 mM phosphate buffer promotes progressive layer interdiffusion with increasing distance from the substrate. However, adding 0.1 M NaCl to the phosphate buffer solution restores the layer stratification. We also find that SA-LbL films obtained from buffer solutions are more stratified as compared to the highly intermixed layers seen in conventional LbL films from buffer. Our results yield new insights into the mechanism of SA-LbL assembly and the final microstructure in comparison with traditional LbL assemblies.

Introduction

Since the earliest work on layer-by-layer (LbL) grown assemblies in the 1990s, the field has become an attractive subject for basic and applied research because of the unique capability to create by this method highly tailored ultrathin materials with nanometer-level control over composition, thickness, and tunable chemical functionality.[1−9] These organized multilayer materials are commonly produced via alternate dipping from aqueous solutions of oppositely charged species (biological molecules, polymers, organic molecules, and nanoparticles) or compounds with hydrogen-bound donor and acceptor groups. Great advances have been made in understanding the fundamental properties and in developing applications for these materials, as highlighted in recent reviews and books.[10−20] Since earlier days, to investigate the internal structure of LbL films at the nanoscale level, scattering techniques such as neutron reflectivity and X-ray reflectivity have been extensively utilized.[21−27] X-ray reflectivity provided valuable information on organic−inorganic LbL films (e.g., via the inclusion of nanoparticles) and on the overall film microstructure (thickness and roughness) but does not resolve the interior organization of polyelectrolyte LbL films with weak electron density contrast. Therefore, one can exploit the neutron scattering contrast between the different isotopes of hydrogen, protium (^{1}H), and deuterium (^{2}H) to label structural features of interest within a polyelectrolyte LbL film in a neutron reflectivity measurement.

Neutron reflectivity was first utilized to study the internal structure of conventional (dipped) LbL films made by the traditional routine of adsorption from solution of strong polyelectrolytes combined with selectively deuterated polyelectrolyte layers.[28−31] In those LbL films, polymer cationic or anionic components with individual layer thicknesses of several nanometers were shown to be partially intermixed, but strong evidence of internal layering was observed in the form of pronounced superlattice peaks in the

† Part of the "Langmuir 25th Year: Self-assembled polyelectrolyte multilayers: structure and function" special issue.

*Corresponding author. E-mail: vladimir@mse.gatech.edu.

(1) *Multilayer Thin Films: Sequential Assembly of Nanocomposite Materials*; Decher, G., Schlenoff, J.B., Eds.; Wiley-VCH: Weinheim, Germany, 2002.
(2) *Macromolecular Engineering, Elements of Macromolecular Structural Control*; Jessel, N., Lavalle, P., Ball, V., Ogier, J., Senger, B., Picart, C., Schaaf, P., Voegel, J.-C., Decher, G., Gnanou, Y., Leibler, L., Matyiaszewski, K., Eds.; Wiley-VCH: Weinheim, Germany, 2007; Vol. *2*, p 1249.
(3) Hiller, J. A.; Mendelsohn, J. D.; Rubner, M. F. *Nat. Mater.* **2002**, *1*, 59.
(4) Schlenoff, J. B.; Rmaile, A. H.; Bucur, C. B. *J. Am. Chem. Soc.* **2008**, *130*, 13589.
(5) Lvov, Y.; Decher, G.; Möhwald, H. *Langmuir* **1993**, *9*, 481.
(6) Lvov, Y.; Ariga, K.; Ichinose, I.; Kunitake, T. *Langmuir* **1996**, *12*, 3038.
(7) Tsukruk, V. V.; Bliznyuk, V. N.; Visser, D. W.; Cambell, A. L.; Bunning, T.; Adams, W. W. *Macromolecules* **1997**, *30*, 6615.
(8) Caruso, F. *Adv. Mater.* **2001**, *13*, 11.
(9) Tsukruk, V. V. *Prog. Polym. Sci.* **1997**, *22*, 247.
(10) Hammond, P. *Adv. Mater.* **2004**, *16*, 1271.
(11) Sukhishvili, S.; Kharlampieva, E.; Izumrudov, V. *Macromolecules* **2006**, *39*, 8873.
(12) Srivastava, S.; Kotov, N. *Acc. Chem. Res.* **2008**, *41*, 1831.
(13) Kharlampieva, E.; Sukhishvili, S. A. *Polym. Rev.* **2006**, *46*, 377.
(14) Tang, Z.; Wang, Y.; Podsiadlo, P.; Kotov, N. A. *Adv. Mater.* **2006**, *18*, 3203.
(15) Klitzing, R.v.; Wong, J. E.; Jaeger, W.; Steitz, R. *Curr. Opin. Colloid Interface Sci.* **2004**, *9*, 158.
(16) Johnston, A. P. R.; Cortez, C.; Angelatos, A. S.; Caruso, F. *Curr. Opin. Colloid Interface Sci.* **2006**, *11*, 203.
(17) *Protein Architecture: Interfacial Molecular Assembly and Immobilization Biotechnology*; Lvov, Y., Möhwald, , H., Eds.; Marcel Dekker: New York, 2000.
(18) Jiang, C.; Tsukruk, V. V. *Adv. Mater.* **2006**, *18*, 829.
(19) Jiang, C.; Tsukruk, V. V. *Soft Matter* **2005**, *1*, 334.
(20) Sukhishvili, S. A. *Curr. Opin. Colloid Interface Sci.* **2005**, *10*, 37.
(21) Klitzing, R. V. *Phys. Chem. Chem. Phys.* **2006**, *8*, 5012.
(22) Decher, G.; Lvov, Y.; Schmitt, J. *Thin Solid Films* **1994**, *244*, 772.
(23) Decher, G.; Hong, J. D.; Schmitt, J. *Thin Soild Films* **1992**, *210*, 831.
(24) Erokhina, S.; Berzina, T.; Cristofolini, L.; Erokhin, V.; Folli, C.; Konovalov, O.; Marino, I.-G.; Fontana, M. P. *Langmuir* **2008**, *24*, 12093.
(25) Glinel, K.; Laschewsky, A.; Jonas, A. M. *J. Phys. Chem. B* **2002**, *106*, 11246.
(26) Jean, B.; Heux, L.; Dubreuil, F.; Chambat, G.; Cousin, F. *Langmuir* **2009**, *25*, 3920.
(27) Bliznyuk, V. N.; Rinderspacher, F.; Tsukruk, V. V. *Polymer* **1998**, *39*, 5249.
(28) Schmitt, J.; Grünewald, T.; Decher, G.; Pershan, P. S.; Kjaer, K.; Lösche, M. *Macromolecules* **1993**, *26*, 7058.
(29) Kellogg, G. J.; Mayes, A. M.; Stockton, W. B.; Ferreira, M.; Rubner, M. F.; Satija, S. K. *Langmuir* **1996**, *12*, 5109.
(30) Lösche, M.; Schmitt, J.; Decher, G.; Bouwman, W. G.; Kjaer, K. *Macromolecules* **1998**, *31*, 8893.
(31) Korneev, D; Lvov, Y; Decher, G; Schmitt, J; Yaradaikin, S. *Physica B: Condens. Matter* **1995**, *213*, 954.

neutron reflectivity profiles. For example, in poly(styrene sulfonate) (PSS) and poly(allylamine hydrochloride) (PAH) films assembled at high salt concentration (>0.5 M) the interlayer roughness between adjacent polyelectrolyte layers was found to be on the order of 1.2−1.6 nm, comprising $\sim 0.4 d_{bl}$, where d_{bl} is the PAH−PSS bilayer thickness indicating well-defined layer structure with intermixing between adjacent layers of the same order as the layer thickness.[28,30] The intensity, width, and wavevector (Q) dependence of the superlattice reflectivity peaks produced by the deuterated marker layers of *d*PSS provide a wealth of information about the quality of layering within the selectively labeled LbL films.

Using neutron reflectivity, well-ordered layered structures were also found in the case of lipid layers[32] or multilayer films made of alternating sheets of rigid cellulose crystals and flexible PAH.[33] Internal layer ordering was shown to be influenced by external parameters such as pH, ionic strength, temperature, and humidity both during deposition and after postassembly treatment.[34−38] For example, increasing ionic strength or temperature during deposition resulted in increased interfacial mixing of PAH−PSS films.[39,40] Schlenoff and co-workers demonstrated that the postassembly exposure of polylectrolyte multilayers to high concentrations of salt (0.8−1 M NaCl) induces a significant increase in polymer interlayer mixing.[41] Neutron reflectivity was also employed to resolve the structure of multilayers composed of weak polyelectrolytes, which exhibit more diffuse polymer layering as compared to strong polyelectrolytes.[42] The multilayer structure of the weak polyelectrolyte films can be made to disappear completely after the pH-induced release of polyacid.[42] Recently, neutron reflectivity was applied to hydrogen-bonded systems of a weak polyelectrolyte and a neutral component where interactions between adjacent layers are controlled solely by hydrogen bonding.[43] That study demonstrated that the structure and properties of hydrogen-bonded films are tightly interconnected and that internal layering strongly correlates with the strength of intermolecular interactions between adjacent molecular layers.

All of the neutron reflectivity studies published to date in this field have focused on multilayer films prepared by a conventional LbL approach (alternating dipping from polymer solutions). Only very recently was neutron reflectivity applied to LbL multilayers constructed via a different assembly approach - a spraying technique[44,45] It was shown that spraying does not dramatically affect the layering quality. However, the sprayed layers were observed to be 30% thinner than conventional dipped LbL films obtained under the same conditions.[45]

An alternative to these LbL depositions is spin-assisted LbL (SA-LbL) assembly, which has been introduced by Char and Wang as a combination of the conventional LbL growth with the spin-coating routine.[46,47] This spin-assisted technique has several advantages over the conventional assembly. First, it offers one the ability to construct organized ultrathin films much more rapidly than by using the traditional methods of LbL assembly and thus is considered to be more "technologically friendly". Second, SA-LbL films have been found to possess remarkable physical properties, such as high mechanical robustness and strength as was demonstrated in our previous studies. On the basis of this assembling technique, a method to obtain flexible free-standing membranes with thicknesses down to 30 nm and lateral dimensions of several centimeters was developed.[18,48−50] The incorporation of metal nanoparticles into SA-LbL films improves the film stability and mechanical properties even further.[51,52] Moreover, these composite robust ultrathin flexible films have shown extraordinary sensitivity and dynamic range in the freely suspended state, with a potential application as a new generation of pressure and temperature sensor arrays.[52−54] Recently, SA-LbL polylectrolyte/titania nanocomposite films that exhibited interesting physical properties have been obtained.[55,56] Finally, SA-LbL offers the incorporation of nonpolar hydrophobic moieties and the layering of complex biological materials, which would be challenging with conventional LbL assembly.[57,58]

Despite the extensive recent use of this method,[59−61] a fundamental understanding of the mechanism of SA-LbL film formation and its true inner microstructure is still in its infancy. It is generally suggested that strong shear forces combined with fast solvent removal in the course of assembly are responsible for the enhanced mechanical integrity of these films, but no direct evidence of stratified organization in these films has been published to date. Char et al. examined the internal structure of nanoparticle-containing SA-LbL films using X-ray reflectivity.[46] To create sufficient electron-density contrast, quantum dots (QD) were incorporated within the polyelectrolyte layers. The authors observed QD layers to be resolved with 5 nm spacing, thus suggesting high level of stratification of these nanoparticles.[46] However, the data obtained for hybrid organic−inorganic systems does not provide a direct view of the polyelectrolyte layering in the absence of inorganic nanoparticles. Neutron reflectivity, which exploits deuterated marker layers, makes possible an accurate analysis of internal structure within all-polymer SA-LbL films.

(32) Delajon, C.; Gutberlet, T.; Steitz, R.; Möhwald, H.; Krastev, R. *Langmuir* **2005**, *21*, 8509.
(33) Jean, B.; Dubreuil, F.; Heux, L.; Cousin, F. *Langmuir* **2008**, *24*, 3452.
(34) Decher, G.; Eckle, M.; Schmitt, J.; Struth, B. *Curr. Opin. Colloid Interface Sci.* **1998**, *3*, 32.
(35) Glinel, K.; Prevot, M.; Krustev, R.; Sukhorukov, G. B.; Jonas, A. M.; Möhwald, H. *Langmuir* **2004**, *20*, 4898.
(36) Carrière, D.; Krastev, R.; Schönhoff, M. *Langmuir* **2004**, *20*, 11456.
(37) Tanchak, O. M.; Yager, K. G.; Fritzsche, H.; Harroun, T.; Katsaras, J.; Barrett, C. J. *Langmuir* **2006**, *22*, 5137.
(38) Kügler, R.; Schmitt, J.; Knoll, W. *Macromol. Chem. Phys.* **2002**, *203*, 413.
(39) Gopinadhan, M.; Ivanova, O.; Ahrens, H.; Günther, J.-U.; Steitz, R.; Helm, C. A. *Macromolecules* **2005**, *38*, 5228.
(40) Gopinadhan, M; Ivanova, O.; Ahrens, H.; Günther, J.-U.; Steitz, R.; Helm, C. A. *J. Phys. Chem. B* **2007**, *111*, 8426.
(41) Jomaa, H. W.; Schlenoff, J. B. *Macromolecules* **2005**, *38*, 8473.
(42) Kharlampieva, E.; Ankner, J. F.; Rubinstein, M.; Sukhishvili, S. A. *Phys. Rev. Lett.* **2008**, *100*, 128303.
(43) Kharlampieva, E.; Kozlovskaya, V.; Ankner, J. F.; Sukhishvili, S. A. *Langmuir* **2008**, *24*, 11346.
(44) Kolasinska, M.; Krastev, R.; Gutberlet, T.; Warszynski, P. *Langmuir* **2009**, *25*, 1224.
(45) Félix, O.; Zheng, Z.; Cousin, F.; Decher, G. *C. R. Chim.* **2009**, *12*, 225.
(46) Cho, J.; Char, K.; Hong, J.-D.; Lee, K.-B. *Adv. Mater.* **2001**, *13*, 1076.
(47) Chiarelli, P. A.; Johal, M. S.; Casson, J. L.; Roberts, J. B.; Robinson, J. M.; Wang, H.-L. *Adv. Mater.* **2001**, *13*, 1167.
(48) Jiang, C.; Markutsya, S.; Tsukruk, V. V. *Adv. Mater.* **2004**, *16*, 157.
(49) Zimnitsky, D.; Shevchenko, V. V.; Tsukruk, V. V. *Langmuir* **2008**, *24*, 5996.
(50) Lin, Y. H.; Jiang, C.; Xu, J.; Lin, Z.; Tsukruk, V. V. *Soft Matter.* **2007**, *3*, 432.
(51) Jiang, C.; Markutsya, S.; Shulha, H.; Tsukruk, V. V. *Adv. Mater.* **2005**, *17*, 1669.
(52) Jiang, C.; Markutsya, S.; Pikus, Y.; Tsukruk, V. *Nat. Mater.* **2004**, *3*, 721.
(53) Jiang, C.; McConney, M. E.; Singamaneni, S.; Merrick, E.; Chen, Y.; Zhao, J.; Zhang, L.; Tsukruk, V. V. *Chem. Mater.* **2006**, *18*, 2632.
(54) Kharlampieva, E.; Slocik, J. M.; Tsukruk, T.; Naik, R. R.; Tsukruk, V. V. *Chem. Mater.* **2008**, *20*, 5822.
(55) Sohn, B.-H.; Kim, T.-H.; Char, K. *Langmuir* **2002**, *18*, 7770.
(56) Kharlampieva, E.; Tsukruk, T.; Slocik, J. M.; Ko, H.; Poulsen, N.; Naik, R. R.; Kroger, N.; Tsukruk, V. V. *Adv. Mater.* **2008**, *20*, 3274.
(57) Lee, S.; Lee, B.; Kim, B. J.; Park, J.; Yoo, M.; Bae, W. K.; Char, K.; Hawker, C. J.; Bang, J.; Cho, J. *J. Am. Chem. Soc.* **2009**, *131*, 2579.
(58) Jiang, C.; Wang, X.; Gunawidjaja, R.; Lin, Y.-H.; Gupta, M. K.; Kaplan, D. L.; Naik, R. R.; Tsukruk, V. V. *Adv. Funct. Mater.* **2007**, *17*, 2229.
(59) Seo, J.; Lutkenhaus, J. L.; Kim, J.; Hammond, P. T.; Char, K. *Langmuir* **2008**, *24*, 7995.
(60) Cho, H.; Jang, H.; Yeom, B.; Kim, H.; Kim, R.; Kim, S.; Char, K.; Caruso, F. *Langmuir* **2006**, *22*, 1356.
(61) Jang, H.; Kim, S.; Char, K. *Langmuir* **2003**, *19*, 3097.

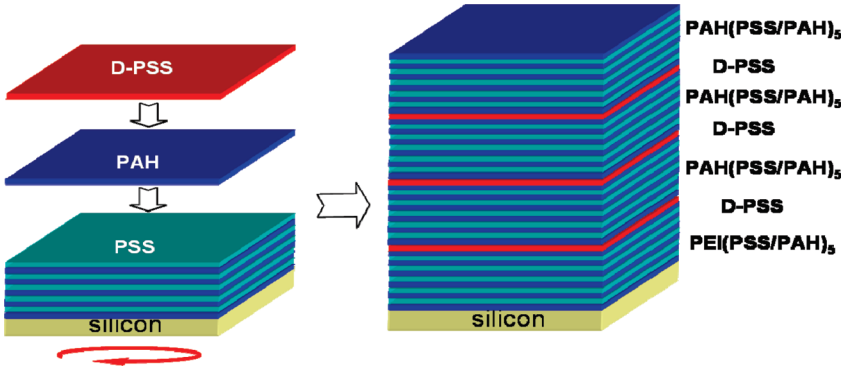

Figure 1. Graphic representation of SA-LbL assembly and the resulting multilayer architecture with selectively labeled *d*PSS layers.

The effect of ionic strength on LbL assembly, an intensively studied topic in the case of conventional LbL films, has not been addressed for recently introduced SA-LbL assemblies. Moreover, all of the studies described above involved SA assembly from salt-free solutions and did not explore ionic strength variation, a powerful parameter for controlling structure and properties in dipped LbL films.[28,41,4] To our knowledge, the effect of ionic strength on SA-LbL film formation remains uncharted to date, probably because of the early nature of studies on SA multilayers. We believe that the ongoing development of the SA-LbL deposition technique as a means to prepare organized nanomaterials rapidly and easily with remarkable mechanical and optical properties requires a molecular-level understanding of their internal structure under variable external conditions. Moreover, the manipulation of the internal structure of SA-LbL films by varying the concentration of phosphate buffer and sodium chloride is relevant to physiological conditions and therefore might be essential for biological applications.

Therefore, in this work, we apply neutron reflectivity to probe the internal structure of SA-LbL films composed of electrostatically assembled PAH−PSS polyelectrolytes. Our results uncover *distinct layering* in SA-LbL films when deposited from salt-free solutions. We find that the degree of molecular intermixing within such films can be controlled by varying the type and concentration of salt in the deposition solutions. Indeed, we demonstrated that the addition of a 10 mM phosphate buffer induces intermixing but the presence of 0.1 M NaCl in the phosphate buffer restores layer stratification. We found that conventional dipped LbL films prepared under identical conditions from buffer solution display a more intermixed internal structure as compared to those made by SA-LbL assembly. To the best of our knowledge, this study presents the first direct observation of the highly stratified internal structure of all-polymer SA-LbL assemblies from salt-free solutions.

Experimental Section

Materials. The weight-average molecular weights (M_w) of deuterated PSS (*d*PSS, Polymer Source) and hydrogenated poly(ethyleneimine) (PEI), PSS, and PAH (Aldrich) were 55, 25, 70, and 60 kDa, respectively. Silicon wafers of 2 in. diameter with one side polished were purchased from the Institute of Electronic Materials Technology (Poland). Nanopure water with a resistivity 18.2 MΩ cm was used in all experiments. To control the pH and ionic strength, 0.1 M HCl, 0.1 M NaOH, and the inorganic salts NaCl and NaH_2PO_4 (Aldrich) were used as received.

Multilayer Deposition. Polyelectrolytes were dissolved in Nanopure water, in 0.01 M phosphate buffer, or in 0.1 M NaCl in 0.01 M monobasic phosphate buffer solutions. The phosphate buffer provided pH 4.8, which was further adjusted to pH 4 with HCl. Salt-free solutions of PAH and PSS had pH values of 3.5 and 5.5, respectively. Prior to film deposition, the silicon wafers were cleaned as described elsewhere[43] and primed with PEI, whose adsorption at pH 4 from 0.01 M phosphate buffer solution for 15 min yielded a monolayer of 2 nm dry thickness. The assembly of 23-bilayer films of PEI[(PSS−PAH)$_5$/*d*PSS/PAH]$_3$(PSS/PAH)$_5$ was then performed from 2 mg/mL solutions by either conventional or SA-LbL deposition.

The conventional LbL procedure involved alternating the immersion of the wafers in polyelectrolyte solutions for 10 min, followed by rinsing twice with Nanopure water or buffer. To perform LbL deposition via the SA method, 3 mL shots of polyelectrolyte solution were sequentially dropped onto a silicon substrate and rotated for 20 s at 3000 rpm on a spin-coater (Laurell Technologies) and then rinsed twice with Nanopure water or buffer followed by the deposition of the next layer.[62] The scheme for deposition was kept identical for all systems: *d*PSS was deposited with every sixth bilayer to provide neutron contrast as illustrated in Figure 1. The samples were dried with dry nitrogen and brought to Oak Ridge National Lab (ORNL) for neutron reflectivity measurements.

Instrumentation. Film morphology was studied with a Dimension 3000 AFM microscope (Digital Instruments). AFM images were collected in light tapping mode with silicon tips with a spring constant of 50 N/m according to the established procedure.[63,64] Ellipsometry measurements of layer thickness were performed with an M2000U (Woolam) spectroscopic ellipsometer.

Neutron Reflectivity. Neutron reflectivity measurements were conducted on dry LbL films at the Spallation Neutron Source Liquids Reflectometer (SNS-LR) at ORNL. The SNS-LR collects specular reflectivity data in a continuous-wavelength band at several different incident angles. For the data presented here, we used the wavelength band of 2 Å $< \lambda <$ 5.5 Å and measured reflectivity at angles of $\theta = 0.15, 0.25, 0.40, 0.75, 1.20,$ and 2.20°, thereby spanning a total wavevector transfer ($Q = (4\pi \sin\theta)/\lambda$) range of 0.006 Å$^{-1} < Q <$ 0.192 Å^{-1}. The data were collected at each angle with incident-beam slits set to maintain the wavevector resolution constant at $\delta Q/Q = 0.05$, which allowed us to stitch the six different angle data sets together into a single reflectivity curve.

The data were analyzed using a model elaborated for conventional polyelectrolyte multilayers, as described previously.[43] To fit the data, we started with an idealized LbL structure featuring sharp interfaces between adjacent layers. This LbL model was then modified by introducing layer-to-layer intermixing to fit our experimental data. The fitting parameters used for all systems are presented in Supporting Information as Tables 1S−4S. In the model, the relative thickness of PSS versus PAH was fixed for any

(62) Markutsya, S.; Jiang, C.; Pikus, Y.; Tsukruk, V. V. *Adv. Funct. Mater.* **2005**, *15*, 771.
(63) Tsukruk, V. V. *Rubber Chem. Technol.* **1997**, *70*, 430.
(64) Tsukruk, V. V.; Reneker, D. H. *Polymer* **1995**, *36*, 1791.

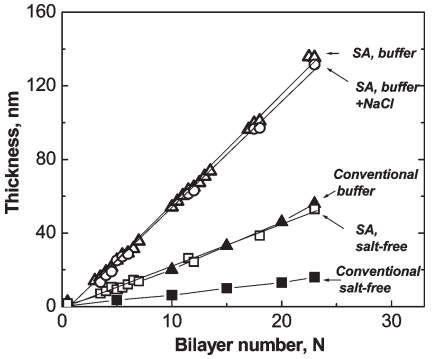

Figure 2. LbL growth of PSS−PAH films assembled by conventional (filled symbols) or SA (open symbols) approaches from salt-free solution (squares), 10 mM phosphate buffer (triangles), or 10 mM phosphate buffer with the addition of 0.1 M NaCl (circles) solutions.

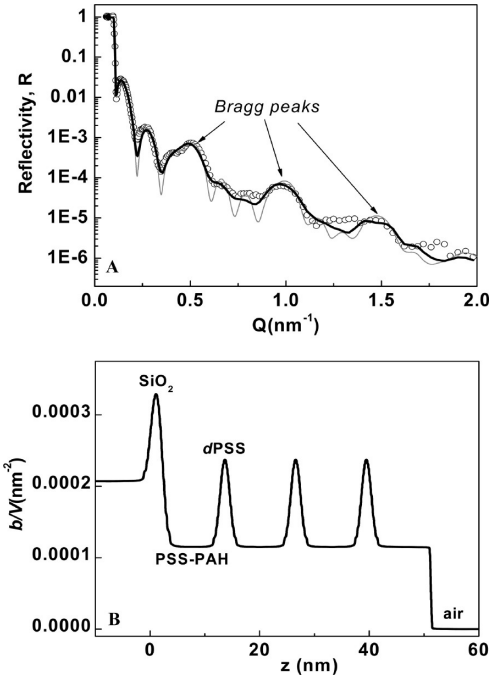

Figure 3. Neutron reflectivity (A) and the corresponding SLD profile (B) for a PEI[(PSS−PAH)$_5$/*d*PSS/PAH]$_3$(PSS/PAH)$_5$ film obtained from salt-free solutions via SA-LbL assembly. Open symbols and solid lines in plot A stand for the experimental data and fit, respectively. The black solid line in the plot A accounts for the thickness variation over the sample surface while holding other model parameters constant. (See the text.) In the profile, these thicker or thinner films would be seen as greater or lesser spacing between deuterated marker *d*PSS layers, which are still equally spaced.

specific system but varied in the different films. Initial individual layer thicknesses for simulations were taken from ellipsometry measurements and then adjusted to correspond to the superlattice peaks in the neutron reflectivity. The calculated reflectivity curves were optimized for the goodness of fit.[43]

The neutron scattering density is defined as $\Sigma = b/V$, where b is the monomer scattering length (sum of the scattering lengths of constituent atomic nuclei) and V is the monomer volume.[43] The scattering contrast between protonated PSS and PAH is insignificant, so we used a thickness-weighted-average protonated layer scattering density Σ_{p_0} for the protonated PSS−PAH bilayers. We observed that, in general, the thicknesses of the *d*PSS marker layers exceeded the nominal total thickness of a PSS−PAH

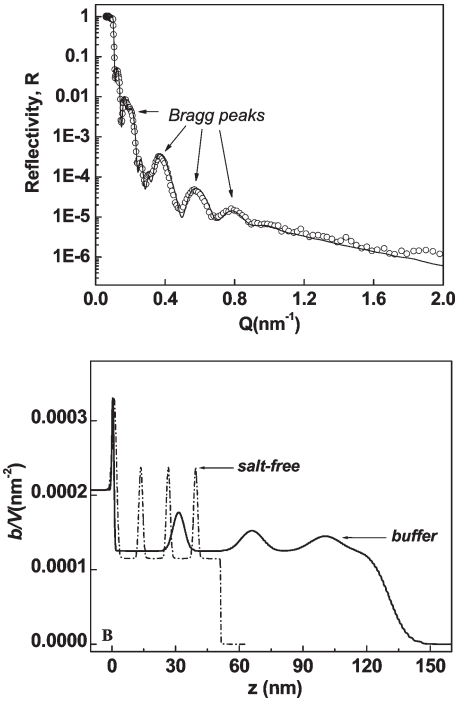

Figure 4. Neutron reflectivity (A) and the corresponding SLD profile (B, solid line) for a PEI[(PSS−PAH)$_5$/*d*PSS/PAH]$_3$(PSS/PAH)$_5$ film obtained from phosphate buffer via SA-LbL assembly. Open symbols and solid line in plot A stand for the experimental data and fit, respectively. The dashed line in plot B shows for comparison the fitted profile for the spin-assisted film prepared from salt-free solutions (Figure 3B).

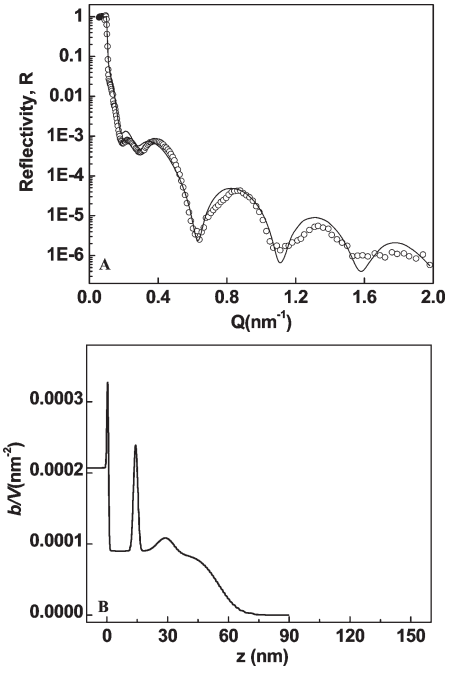

Figure 5. Neutron reflectivity (A) and the corresponding SLD profile (B) for a PEI[(PSS−PAH)$_5$/*d*PSS/PAH]$_3$(PSS/PAH)$_5$ film obtained from phosphate buffer via conventional assembly. Open symbols and the solid line in plot A stand for the experimental data and fit, respectively.

bilayer, implying a large amount of intermixing between layers. We accounted for mass balance within these diffuse *d*PSS layers, which is equivalent to keeping the amount of deuterated material

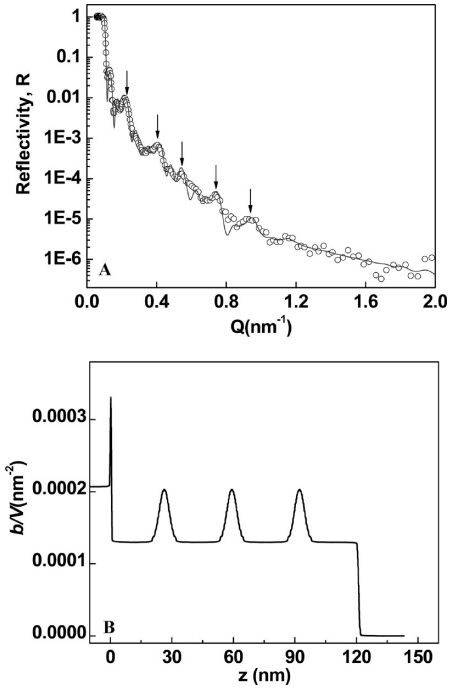

Figure 6. Neutron reflectivity (A) and the corresponding SLD profile (B) for a PEI[(PSS−PAH)$_5$/*d*PSS/PAH]$_3$(PSS/PAH)$_5$ film obtained from phosphate buffer in the presence of 0.1 M NaCl salt solutions via SA-LbL assembly. Open symbols and the solid line in plot A stand for the experimental data and fit, respectively. Bragg peaks in plot A are marked with the arrows.

constant in the model. The amount of deuterated material is proportional to the difference in scattering density between the pure deuterated layer and the protonated background multiplied by the nominal thickness of the pure deuterated layer: $M_{d_0}=(\Sigma_{d_0}-\Sigma_{p0})\times d_{d_0}$, where Σ_{d_0} is the *d*PSS bulk scattering density and d_{d_0} the nominal deuterated marker layer thickness. The quantity M_{d0} is thus invariant in the model. Distributing deuterated material over a greater thickness d_d can only be done by mixing the original deuterated layer with the surrounding protonated matrix. Because M_{d_0} must remain constant, the scattering density of a diffuse layer of thickness d_d is constrained to be $\Sigma_d = M_{d_0}/d_d + \Sigma_{p_0}$.

Layer intermixing was simulated by error function density profiles (Gaussian roughness).[41] For the marker layers, the interfacial mixing full width at half maximum (FWHM) σ_d of adjacent interfaces was held equal to the layer thickness d_d. (We found that smaller σ_d values consistently degraded the goodness of fit.) Assuming $\sigma_d = d_d$ is consistent with classical treatments of diffusion from a slab.[65] Most significantly, because substrates and surfaces for our systems are similar, by linking both scattering density and interfacial diffusion to d_d we effectively reduced the number of adjustable parameters in the model. When the deuterated marker layer mixing with the surrounding material becomes so large that adjacent marker layers begin to interact, diffusion is modeled by holding the deuterated marker and protonated background thicknesses equal ($d_p = d_d$) and uniformly decreasing the layer contrast ($\Sigma_d - \Sigma_p$).

In addition to layer intermixing, several of the films exhibited nonuniform layer thickness across the sample surface. This phenomenon appears as a systematic underestimation by modeled reflectivity curves at fringe minima and a broadening of superlattice Bragg peaks that increases with scattering vector *Q*. Where this effect is modest, as in Figures 5 and 6, there is not strong justification for adding additional complexity to the model. When, as in Figure 3, this effect is too large to ignore, we employ an incoherent sum of reflectivity curves calculated for different PSS−PAH bilayer thicknesses to account for the possible minor nonuniformity of LbL films across the large 2-in.-diameter surface of the wafers. Other structural parameters in the model are kept constant. A simple three-thickness model suffices to produce the minima and peak smearing seen in the data: $R_{\text{model}} = (R_{d_0-\Delta d} + 2R_{d_0} + R_{d_0+\Delta d})/4$, where R_d is the specular reflectivity calculated for a PSS/PAH bilayer spacing of *d*. The average bilayer spacing d_0 and other structural parameters are determined by fitting the superlattice and Kiessig fringe peaks in the data. The FWHM of this simple bilayer-spacing distribution, $2\Delta d$, is determined by maximizing the goodness of fit of the minima and peak broadening.

(65) Crank, J. *The Mathematics of Diffusion*, 2nd ed.; Clarendon Press: Oxford, England, 1975.

Table 1. Film Parameters Found from Neutron Reflectivity (Total Film Thickness, Bilayer Thickness, and Internal and External Roughness) and from AFM Images

PAH−PSS system	total film thickness, nm	bilayer thickness, nm	σ_d, nm	σ_{ext}, nm	AFM roughness, nm
SA-LbL in salt-free solutions	49	2.0	1.6	0.3	0.3 ± 0.02
SA-LbL in buffer	129	5.3	5−13	16	12.0 ± 2
SA-LbL in buffer plus salt	120	5.0	4.5	1.0	1.0 ± 0.2
conventional LbL in buffer	54	2.2	1.9−7.4	18	25.0 ± 5

Results

To investigate the effect of salt on SA-LbL film structure, multilayers were deposited from polymer solutions without additional salt, in 10 mM phosphate buffer, and in the phosphate buffer in the presence of 0.1 M NaCl.

Overall Thickness of SA-LbL Films. SA-LbL films prepared from salt-free, buffer, and buffer-plus-salt solutions demonstrated linear growth with an increment per individual bilayer of 2.2, 5.6, and 5.3 nm, respectively (Figure 2). In contrast, conventional LbL films showed much thinner bilayers of 0.6 and 2.2 nm for salt-free and buffer conditions, respectively (Figure 2). Similar differences in thickness were observed in earlier studies, which showed that SA PAH−PSS films prepared from salt-free solution were about 3-fold thicker than conventional films obtained using the same solutions.[46,47]

Internal Structure of Salt-Free SA-LbL Films. The LbL film thicknesses and internal and external roughnesses found from neutron reflectivity are summarized in Table 1. Note that the average bilayer thicknesses measured by neutron reflectivity were found to be 2.0, 5.3, and 5.0 nm for the SA-LbL films obtained in salt-free water, buffer, and buffer plus salt, respectively, which agrees within ±5% with the corresponding bilayers thicknesses derived from the ellipsometry data (Figure 2).

Neutron reflectivity, *R*, for the SA-LbL film prepared from a salt-free solution is shown in Figure 3. In this Figure, *R* is plotted as a function of momentum transfer, *Q* [$(Q = (4\pi \sin\theta)/\lambda)$, where θ is the neutron incident angle and λ is the neutron wavelength], for the SA-LbL films obtained from salt-free solutions, which do not contain small ions supplied by external buffer or salt. The distinct and periodic Bragg peaks observed in this case indicate a high degree of stratification. The scattering-length-density (SLD) profile reveals the sharply contrasting and well-defined natural silicon oxide layer at the surface of the Si crystal, followed by the polymer layers (Figure 3B). The SLD profile also reveals a sequence of three equally spaced labeled *d*PSS layers with thickness (d_d) and scattering length density (Σ_d) equal to 1.6 nm

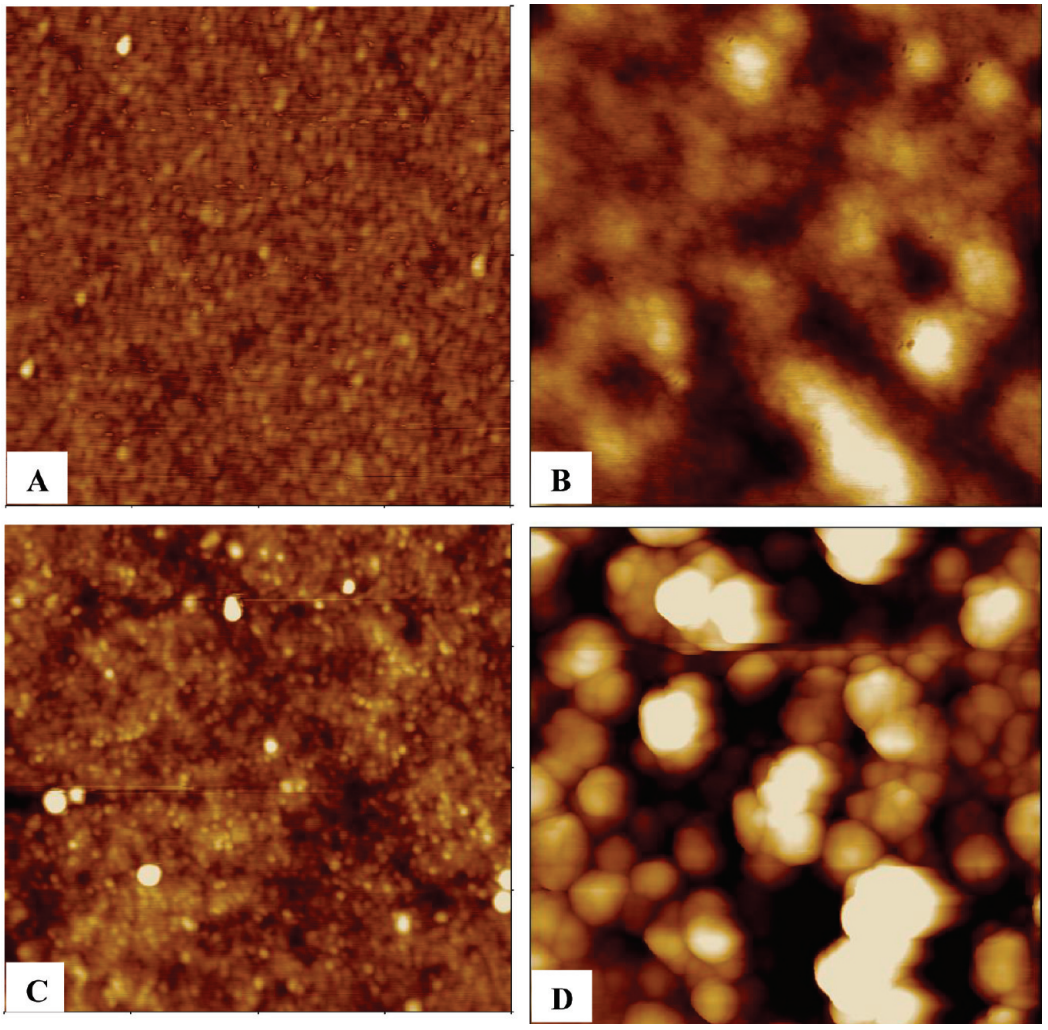

Figure 7. AFM topographical images (A−C) of SA-LbL films obtained from salt-free (A), buffer (B), and buffer-plus-salt solutions (C) and (D) of the conventional LbL film from buffer. The scan area in all cases is 1×1 μm^2 and the heights are 5 nm (A), 20 nm (B), 10 nm (C), and 100 nm (D).

and 2.7×10^{-4} nm^{-2}, respectively (Table 1S in Supporting Information). The marker layers are distinct and do not vary with distance from the substrate, with five bilayers of intervening protonated material (11 nm distance between markers). At the same time, the surface (external) roughness for the film is significantly lower ($\sigma_{ext} = 0.3 \pm 0.2$ nm) than the corresponding internal roughness ($\sigma_d = 1.6$ nm) (Table 1). Apparently, this sample exhibits layer-thickness variation over the sample surface, which we accounted for by introducing a distribution of PSS/PAH bilayer spacings as described above such that the total film thickness varies as 49.1 ± 3.5 nm. In contrast, a conventional dipped LbL film drawn from salt-free solutions featured a very small bilayer thickness (0.6 nm per bilayer) in the ellipsometry measurements (Figure 2). Correspondingly, no superlattice ordering was seen in the neutron reflectivity in this case (Figure 1S).

Interior Structure of SA-LbL Films Prepared from Buffer. SA-LbL deposition from a 10 mM phosphate buffer significantly changes the film internal structure, as manifested by the shift in superlattice peak positions indicating an increase in the bilayer thickness to 5.3 nm as compared to the 2 nm bilayer thickness for the salt-free film (Table 1, Figure 4). Moreover, the neutron reflectivity reveals broadened Bragg peaks indicating more interdiffused layers. In this case, no satisfactory fit of the neutron reflectivity could be obtained unless we suggested that *d*PSS layers were significantly diluted with hydrogenated counterparts. In addition, such dilution consistently increases with the *d*PSS layer number. The SLD profile demonstrates that the labeled peaks are still resolved but that layering decays significantly with increasing distance from the substrate, as manifested in gradual peak broadening and decreasing amplitude (Figure 4B). Specifically, d_d in the sequence of three marker layers increases with distance from the substrate to 5, 9.5, and 13 nm for the first, second, and third *d*PSS layers, respectively (Table 2S in Supporting Information). Correspondingly, layer interdiffusion consistently increases from the bottom to the top of the LbL film and achieves its highest value at the film−air interface of 16 nm (σ_{ext}).

Interior Structure of Conventional LbL Films Prepared from Buffer. A conventional LbL film grown from buffer solution is shown in Figure 5. The film possesses very significant layer interdiffusion in contrast to its SA-LbL counterpart. Well-defined layering is observed only in the part of the film closest to the substrate, followed by a total loss of layering with increasing distance from the substrate. Only two labeled layers can be recognized: a pronounced peak for the first *d*PSS marker ($d_d =$ 1.9 nm) followed by a broad second peak ($d_d = 7.4$ nm) indicating significant intermixing with the hydrogenated material (Table 3S in Supporting Information). The absence of the third labeled *d*PSS peak in the reflectivity profile reveals complete mixing of the adjacent layers. In this case, $\sigma_{ext} = 18$ nm, which is the highest value among all systems studied here (Table 1). Another

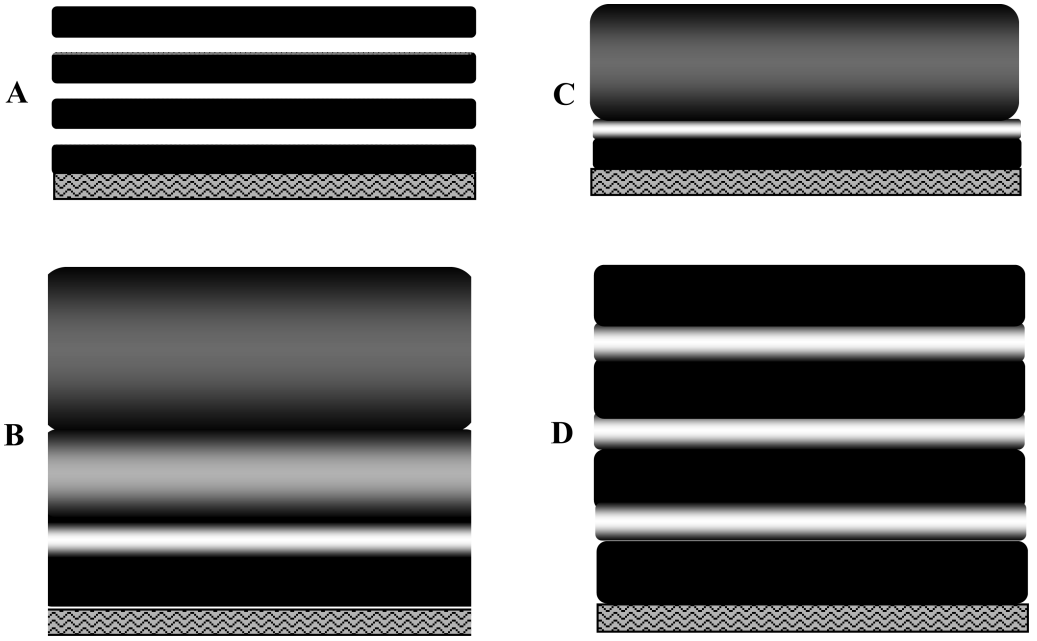

Figure 8. Graphic representation of film architecture obtained by SA-LbL assembly from salt-free (A), phosphate buffer (B), and buffer-plus-salt solutions (D) or by conventional LbL assembly from salt-free solutions (C). White stripes in the scheme stand for *d*PSS. A and D represent stratified multilayer structures; B shows a multilayer with gradually dissipating layering; and C illustrates an interdiffused structure with the layering preserved only in the deuterated stratum closest to the substrate.

observation is that the conventional LbL film is about 3-fold thinner than the SA-LbL film (2.2 vs 5.3 nm), in accordance with the data from ellipsometric measurements.

Interior Structure of SA-LbL Films Prepared from Buffer-Plus-Salt Solutions. An interesting phenomenon was observed when 0.1 M NaCl was added to the 10 mM phosphate buffer. Surprisingly, neutron reflectivity shows that the internal layering in an SA-LbL film is restored under these conditions (Figure 6). The layering in the NaCl buffer solution is persistent at d_d = 4.5 nm, which is in contrast to gradually increasing and generally larger interdiffusion observed in buffer without salt. The values for both internal and external roughness (σ_{ext} = 1 nm and σ_d = 4.5 nm) became much smaller, indicating stratification induced by the salt addition. At the same time, the addition of NaCl results in a 10% decrease in film thickness as compared to that for the SA-LbL film deposited from buffer (Table 1).

Surface Morphology. AFM was applied to verify the surface morphology of the LbL films (Figure 7). All LbL films studied here possessed relatively smooth, uniform surfaces over large surface areas without any indication of large microscale defects, a common feature of LbL films.[7] The surface microroughness of LbL films calculated for $10 \times 10\ \mu m^2$ surface areas correlates well with σ_{ext} values found from neutron reflectivity (Table 1). The SA-LbL films obtained by SA deposition from water and from buffer-plus-salt solutions showed the smoothest surfaces with molecular-level microroughnesses of 0.30 ± 0.02 and 1.0 ± 0.2 nm, respectively (Figure 7). In contrast, LbL films prepared from buffer showed microroughnesses of 12 ± 2 and 25 ± 5 nm for LbL films made by SA and conventional LbL, respectively.

General Discussion

The neutron reflectivity studies conducted here revealed several interesting phenomena. First, SA-LbL films are thicker than those obtained by conventional LbL under the same conditions. Second, the addition of phosphate buffer results in an increase in film thickness for both SA and conventional LbL films but induces significant layer intermixing in SA-LbL films. The stratification in SA-LbL films can then be restored in the presence of NaCl in phosphate buffer solutions. Finally, the SA-LbL films made from buffer display a better-resolved layered structure than the conventional LbL films grown from the buffer. These effects are summarized in Figure 8 and will be discussed below in detail.

Salt-Free LbL Assembly. Our first observation is that the SA-LbL film deposited from salt-free solutions has the most persistent layering with the least internal mixing (σ_d = 1.6 nm) and a molecularly smooth surface (σ_{ext} = 0.30 ± 0.02 nm) (Figure 8a). In this case, $\sigma_d \ll 2R_g$ (~8 nm), where R_g is the estimated radius of gyration for *d*PSS chains (M_w = 55 kDa) in solution assuming a persistence length of 1 nm.[15] The result indicate that the *d*PSS chains are very flat with minimal chain intermixing due to strong ionic binding with adjacent PAH layers.

In fact, a well-defined layer structure with σ_d < 2 nm was earlier observed for conventional or sprayed PSS−PAH films assembled at high ionic strength with a range of salt concentrations from 0.15 to 3 M NaCl.[28,30,41,44,45] Usually, the salt was added to the dipping solutions to obtain thicker films to be resolved with neutron reflectivity. In contrast, SA-LbL assembly allows one to obtain well-layered LbL films without any additional salt in solution. Apparently, in conventional LbL dipping deposition the absence of salt promotes very thin polyelectrolytes layers due to mostly uncoiled chain conformations on the surfaces with chain segment repulsion caused by a lack of charge screening. Thus, conventional LbL films dipped from salt-free solutions show incomplete bilayers of 0.6 nm thickness, which correlates well with the previously found value of 0.8 nm for PSS−PAH bilayers.[30] In contrast, SA-LbL films obtained under identical conditions are ~3-fold thicker than conventional films, as was seen in the Results section. The increased thickness of SA electrostatically bound LbL films was attributed to the fast removal of water during spinning, which facilitates intermolecular binding and minimizes long-range chain-to-chain repulsions.[46] However, a direct comparison of the internal structures of the salt-free SA-LbL film with those made by conventional LbL could not

be made because of the lack of contrast in the latter case when the bilayer thickness was below 1 nm (Figure 1S).

LbL Assembly from Buffer. The significant increase in SA-LbL film thickness in phosphate buffer as illustrated in Figure 8b can be explained by invoking "screened polymer chains" in the presence of small ions.[15] The increase in film thickness with increasing salt concentration is a common feature of conventional LbL films. Adding salt results in partial intrachain charge screening and thus the formation of loopy structures on the surface and thicker layers with high interfacial roughness.[66] In addition, salt favors adsorption because of reduced interchain repulsion. For example, it was shown that the thickness of PSS−PAH films increases from 0.6 to 3 nm per bilayer with increasing salt concentration from 0 to 3 M.[30] In our case, SA-LbL films showed an ~3-fold thickness increase in buffer as compared to salt-free films, which indicates that SA-LbL assembly follows the same trend as conventional LbL assembly in salt solutions.

The phosphate buffer also makes the interior structure of SA-LbL film less stratified (Figure 8b), with layer intermixing persistently increasing with distance from the substrate in spite of the fact that chains show linear film growth and therefore should still be strongly associated. This gradual increase of intermixing with increasing distance from the substrate was found earlier in weak polyelectrolyte and hydrogen-bonded LbL films when the less strongly bound polyelectrolyte pairs had higher interlayer interdiffusion and therefore were found to be less stratified.[29,42,43] In addition, more loosely packed outer layers were observed in multilayers of strong polyelectrolytes.[1,2,4,15] The substrate-mediated layering within the LbL film was explained by stronger chain expansion with increasing layer number, driven by an increase in the chain entropy.[43] Mayes et al. also showed the broadening of labeled PAH−PSS layers obtained from salt-free solutions.[29] In the latter case, interface roughness (σ_d) gradually increased with increasing layer number n as $\sigma_d = (16 + 0.7n)$. In contrast, when 0.5 M NaCl was used for conventional or sprayed LbL film construction, well-resolved, equally spaced layers were obtained with intermixing of layers on the order of the layer thickness ($\sigma_d \approx 1.5$ nm).[30,45]

We suggest that in our case the enhanced layer intermixing is a result of weakening chain-to-chain interactions induced by phosphate buffer. The phenomenon can be explained by the ability of phosphate ions to interact specifically with primary amino groups[67,68] Indeed, the phosphate−PAH interaction results in the partial neutralization of positively charged PAH segments and the formation of a loopy structure upon chain adsorption. We suggest that this accumulation of phosphate ions on the PAH chains weakens the binding of adjacent PAH−PSS layers and results in layer diffusion during deposition.

Interestingly, the intermixing induced by the phosphate buffer is much more severe in the conventional LbL films as compared to that in the SA-LbL films assembled under identical conditions (Figure 8c,b). In the SA-LbL films, the layering is more persistent and features a moderate increase in interfacial mixing for all three marker layers. In contrast, the conventional LbL films in buffer show layering only for the substrate-adjacent region, followed by total intermixing in the vicinity of the film−air interface (Figure 8c). Thus, we can conclude that the SA process significantly enhances interlayer interactions, which leads to a well -organized internal structure. Apparently, under shear the polymer chains are kinetically trapped when forming contacts with the surface within a limited time allowed for chain reorganization due to fast solvent removal.[46,59,69] The effect results in decreased roughness and improved stratification of polyelectrolyte layers.

Effect of NaCl on Internal Film Structure. A drastic difference in internal layering is observed when NaCl is added to the phosphate buffer. Instead of the gradual decay in layering observed in the SA-LbL films prepared from buffer, well-resolved, equally spaced dPSS layers appeared again (Figure 8d). In this case, σ_d (4.5 nm) > σ_{ext} (1.6 nm), similar to that observed earlier for the conventional LbL films obtained in 1 M KCl showing values of 1.9 and 1.3 nm for σ_d and $\sigma_{ext,}$ respectively.[28] The larger σ_d observed in our case can be explained by the presence of phosphate buffer as discussed above. We suggest that the better stratification in buffer-plus-salt solutions as compared to that in buffer might be explained by the replacement of the phosphate ions bound to PAH chains in solutions with chloride ions. Such replacement makes the PAH chains available for stronger interaction with PSS, which results in preferred layering. At the same time, the presence of NaCl in the phosphate buffer did not affect the film thickness and layering significantly. Only a slight decrease in thickness (~10%) was observed for SA-LbL films in buffer-plus-salt solutions as compared to that for the films in buffer.

Conclusions

We observed, for the first time, highly stratified structure with well-defined layering in SA-LbL films obtained from salt-free solutions. However, the internal structure can be drastically changed from stratified to interdiffused in the presence of a small concentration of phosphate ions (10 mM) and in turn changed back to a highly stratified structure by adding NaCl to the buffer solution during deposition. Moreover, the presence of phosphate buffer affects the structure by increasing the degree of interdiffusion. At the same time, the SA-LbL films deposited from buffer show more persistent layering than conventional LbL films. We also found that introducing NaCl into the phosphate buffer increases the internal and external roughness of the SA-LbL films as compared to those for salt-free films. Finally, the presence of NaCl in the phosphate buffer during LbL film construction allows one to obtain stratified films that are thicker than those made from salt-free solutions.

Thus, we have demonstrated that the degree of polyelectrolyte intermixing in SA-LbL films can be tuned by type and concentration of salt in the deposition solutions. The increasing interest in SA-LbL assembly requires a rational film design based upon a fundamental understanding of the relationship between internal structure and fabrication conditions. We believe that gaining insight into the mechanism of SA-LbL assembly and control over the resulting film structure allows rational control of film microstructure and characteristics, which is essential for their applications as sophisticated functionalized nanomaterials.

Acknowledgment. This work was supported by funding provided by the Air Office of Scientific Research FA9550-08-1-0446 project, grant NSF-CBET-NIRT 0650705, and the DOE (under contract DE-AC05-00OR22725).

Supporting Information Available: Model parameters and neutron reflectivity data for PEI[(PSS−PAH)$_5$/dPSS/PAH]$_3$(PSS/PAH)$_5$ films. Effect of substrate size on the structure of spin-assisted LbL films. This material is available free of charge via the Internet at http://pubs.acs.org.

(66) McAloney, R. A.; Sinyor, M.; Dudnik, V.; Goh, M. C. *Langmuir* **2001**, *17*, 6655.
(67) Kovačević, D.; van der Burgh, S.; de Keizer, A.; Cohen Stuart, M. A. *J. Phys. Chem. B* **2003**, *107*, 7998.
(68) Irigoyen, J.; Moya, S. E.; Iturri, J. J.; Llarena, I.; Azzarony, O.; Donath, E. *Langmuir* **2009**, *25*, 3374.
(69) Hong, H.; Steiz, R.; Kirstein, S.; Davidov, D. *Adv. Mater.* **1998**, *10*, 1104.